Dyes and Pigments 226 (2024) 112149

Contents lists available at ScienceDirect

Dyes and Pigments

journal homepage: www.elsevier.com/locate/dyepig

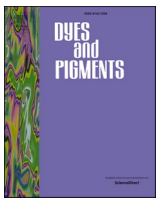

Color modulation in organometallic dyes. Purple-colored acyclic carbenes derived from 2-isocyanoazulene gold(I) complexes

Estela de Domingo, Manuel Bardají, Gregorio García, Silverio Coco *

IU CINQUIMA/Química Inorgánica, Facultad de Ciencias, Universidad de Valladolid, 47071, Valladolid, Spain

ARTICLE INFO

Keywords:
Azulene
Carbene
Dye
Gold
DFT
Organometallic

ABSTRACT

This study reports new carbene azulene gold(I) complexes [AuCl{C(NHAz)(NR_2)}] (R = Me (**1**) and ^{n}Bu (**2**)) and [Au($C_6F_4OC_{10}H_{21}$){C(NHAz)(NR_2)}] (R = Me (**3**) and ^{n}Bu (**4**)) prepared by reaction of 2-isocyanoazulene gold(I) complexes [AuX(CNAz)] (X = Cl and $C_6F_4OC_{10}H_{21}$) with the corresponding secondary amines. Their photophysical properties were investigated by absorption and emission spectroscopies, and by TD-DFT calculations. All the compounds display an intense coloration based on HOMO-LUMO transitions, dominated by the azulene core. Gold-isocyanide complexes show a slight bathochromic shift related to azulene, while a hypsochromic shift was observed after formation of carbene complexes. Thus, the transformation of the gold-isocyanide group into the gold-carbene functionality produces a substantial color change from blue to deep purple. This different electronic behavior is mainly due to the stabilization of the LUMO orbital in the isocyanide complexes, and to the stabilization of the HOMO in the carbene derivatives. These carbene gold complexes show fluorescence in solution associated with the azulene core. This work illustrates how the synthetically easy isocyanide-carbene transformation open new perspectives to a fine color modulation in organometallic azulene dyes.

1. Introduction

Azulene is a 10-π-electron isomer of naphthalene with a large permanent dipole moment of 1.08 D related to the resonance delocalization of azulene, which shows an electron-poor seven-membered ring and an electron rich five-membered ring [1]. Many studies show that azulene derivatives display interesting physical and chemical properties, making them an interesting building block for colorimetric sensors [2–4], stimuli-responsive photo-switches [5], stimuli-responsive for imaging [6], advanced materials for optoelectronic [7–10], nonlinear optical materials [11,12], photovoltaic cells [13,14], and liquid crystals [15–20]. They are also used in cosmetics, baby skincare products, as well as in numerous biomedical applications due to their antioxidant and anti-inflammatory effects [21].

Their properties can be modulated through the tailoring of the azulene core with a variety of functional groups, which have a pronounced influence on the electronic and optical properties of these systems. There are many reports on the effects of introducing different types of organic substituents in different positions of the azulene core and the structure/property relationship is relatively well established, particularly concerning color and emission behavior [1,10,22–29]. Metal-organic substituents have also been used for this purpose, but the number of reports is much lower. There are a few complexes involving multi-hapto coordination of the azulenic framework to the metal [30–33], azuliporphyrin derivatives [34–41], and some isocyanoazulene complexes [42–47]. In this sense, we have recently reported blue dyes based on 2-isocyanoazulene gold(I) complexes [AuX(CNAz)] (Az = azulene; X = halide, perhalophenyl), which display mesomorphic behavior when they contain long substituents [48].

Among the rich diversity of functional groups that can act as ligands to form metal complexes, acyclic diaminocarbenes (ADCs) [49], which can be easily synthesized via metal-templated addition of protic nitrogen nucleophiles to isocyanides [50], constitute an excellent kind of scaffolding efficiently employed as a ligand in gold compounds with applications in catalysis [51–56], medicine [57–60], and optical materials [61,62]. Surprisingly, to date and to the best of our knowledge, the great potential of the diaminocarbene functionality has not been used to modulate the properties of azulene systems.

On these grounds, we decided to extend our initial study on isocyano azulene gold(I) complexes to carbene derivatives. We report here a series of acyclic carbene azulene gold(I) complexes prepared by the synthetic methodology of the nucleophilic attack of amines to isocyano

* Corresponding author.
E-mail address: silverio.coco@uva.es (S. Coco).

https://doi.org/10.1016/j.dyepig.2024.112149
Received 30 January 2024; Received in revised form 10 April 2024; Accepted 11 April 2024
Available online 15 April 2024

azulene gold(I) complexes. We have studied in depth their optical properties, particularly their intense purple color and emission properties. In contrast to the bathochromic shift observed in the electronic spectra when functionalizing azulene with the gold-isocyanide moiety, the introduction of the gold-carbene fragment in the azulene system produces the opposite effect. These results reveal a different electron donor/acceptor character of the isocyanide-gold and the carbene-gold fragments as substituents in the 2-position of the azulene molecule.

2. Results and discussion

2.1. Synthesis and characterization

The N-acyclic carbene azulene gold(I) complexes [AuCl{C(NHAz)(NR_2)}] (R = Me (**1**) and ^{n}Bu (**2**)) and [Au($C_6F_4OC_{10}H_{21}$){C(NHAz)(NR_2)}] (R = Me (**3**) and ^{n}Bu (**4**)) were prepared from the corresponding gold isocyanide complexes by nucleophilic attack of the appropriate amine to the *α*-carbon atom of the coordinated isocyanide, as reported for similar compounds [51] (Scheme 1).

The gold(I) compounds were isolated in good yield, as air-stable purple solids. C, H, N analyses, yields, MALDI-TOF mass spectra, and ^{1}H, ^{19}F and ^{13}C NMR spectroscopic data for the complexes are given in the Experimental Section.

The IR spectra shows the typical carbene bands at 3255-3384 cm^{-1} for *ν*(N–H), and at 1510-1550 cm^{-1} for *ν*(C═N) (overlapped with azulene bands), instead of the *ν*(C ≡ N) band at *ca.* 2200 cm^{-1}, typical of coordinated isocyanide. The ^{1}H NMR spectra show the characteristic pattern of the azulene group, similar to that of the free isocyanide ligand [45]. In addition, a broad singlet is observed in the range 7.89–8.08 ppm (NH), as well as non-equivalent Me or ^{n}Bu resonances. The ^{19}F NMR spectra of the fluorophenyl derivatives **3**–**4** display the typical pattern of two pseudodoublets from an AA'XX' spin system with $J_{AA'} \approx J_{XX'}$, at *ca.* −117.7 (F_{ortho}) and −157.4 ppm (F_{meta}).

In these acyclic N-carbenes, because of the restriction to rotation about the carbene C–N bond (which has considerable multiple character), two isomers are possible (Fig. 1) depending on the arrangement of the azulene group relative to the gold substituent. However, only one isomer was observed in the ^{1}H NMR spectra at room temperature. A nuclear Overhauser effect (NOE) between the NH-carbene (7.9–8.2 ppm) and the NCH_3 or NCH_2 (^{n}Bu) groups supports the less hindered isomer A (Fig. 2).

All the carbene complexes melt directly to an isotropic liquid at low temperatures, particularly the n-butyl derivatives **2** and **4** that bear a long alkoxy substituent (24 and 70 °C, respectively). Consequently, in contrast to the corresponding isocyanide complexes, none shows liquid crystal behavior. Most likely this behavior is associated to the higher molecular width of the carbene molecules compared with the isocyanide compounds.

3. Photophysical studies

The UV–Vis absorption spectra of in dichloromethane (10^{-5} M) of azulene, the isocyanide gold precursors and carbene complexes **1**–**4** are shown in Table 1, and Fig. 3 and S19 (Supplementary Data).

All the electronic absorption spectra are very similar and show a spectral pattern with typical absorption bands and extinction coefficients of the azulene group. The spectra are dominated by highly intense absorption bands in the UV region, with maxima from 280 to 306 nm, and a second set of intense absorption bands also in the UV region with maxima in the range 328–381 nm. In addition, in the visible region, the spectra display a weak and structured absorption band with wavelength maxima at 592 and 601 nm for the isocyanide gold compounds, but from 538 to 541 nm for the carbene gold complexes **1**–**4**, which is assigned to the HOMO → LUMO excitation [45]. For azulene

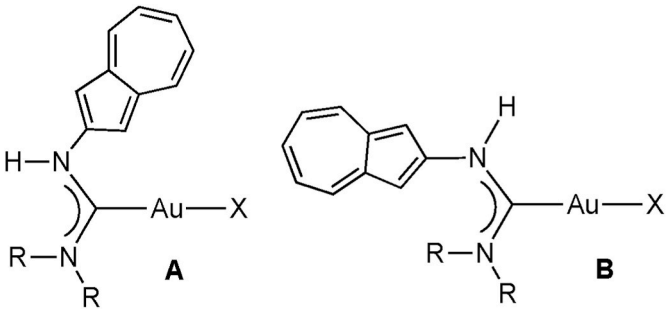

Fig. 1. A and B stereoisomers for carbene gold(I) complexes.

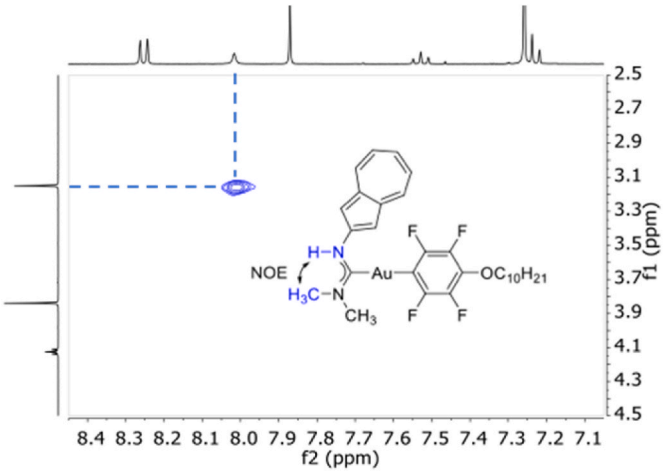

Fig. 2. ^{1}H–^{1}H NOESY 2D NMR of complex [Au($C_6F_4OC_{10}H_{21}$){C(NHAz)(NMe_2)}] (**3**).

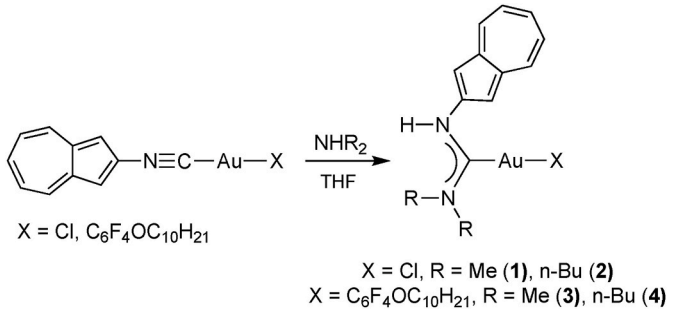

Scheme 1. Synthesis of carbene azulene gold(I) complexes.

Table 1
UV–Visible absorption data for [AuX(CNAz)] (X = Cl, $C_6F_4OC_{10}H_{21}$), [AuCl{C(NHAz)(NR_2)}] (R = Me (**1**) and ^{n}Bu (**2**)) and [Au($C_6F_4OC_{10}H_{21}$){C(NHAz)(NR_2)}] (R = Me (**3**) and ^{n}Bu (**4**)) in dichloromethane (10^{-5} M) at 298 K.

Compound	λ(nm) (10^{-3} *ε*)/dm^3 mol^{-1} cm^{-1}
[AuCl(CNAz)]	657[a] (0.2), 592 (0.7), 567 (0.6), 357 (13.6), 340 (8.8), 333 (8.4), 296 (74.4), 287 (67.8)
[Au(TFP)(CNAz)][b]	656[a] (0.3), 601 (0.7), 564 (0.7), 357 (17.7), 341 (11.6), 333 (11.2), 296 (70.7), 288 (68.2)
1	624[a] (0.1), 576 (0.3), 541 (0.4), 379 (12.5), 363 (9.5), 349 (7.1), 303 (80.0), 294 (64.6)
2	626[a] (0.2), 576 (0.5), 539 (0.6), 381 (13.8), 364 (9.8), 343 (6.0), 305 (82.5), 292 (66.0)
3	628[a] (0.3), 576 (0.5), 541 (0.5), 382 (14.3), 365 (10.0), 349 (7.0), 305 (78.8), 296 (64.0)
4	625[a] (0.2), 573 (0.5), 538 (0.6), 381 (15.4), 367 (11.0), 349 (7.0), 306 (82.3), 298 (66.0)

[a] Shoulder.
[b] TFP: $C_6F_4OC_{10}H_{21}$.

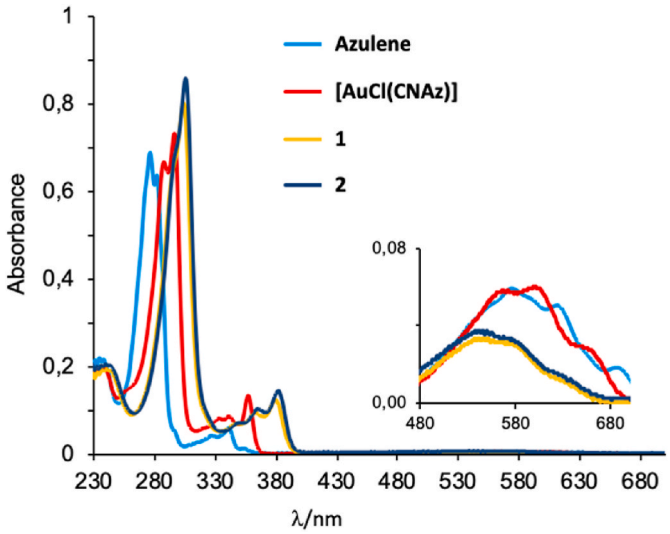

Fig. 3. Selected absorption spectra recorded in CH_2Cl_2 solution (10^{-5} M) at room temperature. Inset: enlargement of absorption in the visible region (10^{-4} M).

itself this transition occurs at λ_{max} 576 nm in dichloromethane (Fig. 3), therefore the functionalization of the azulene molecule in the position 2 with an [-NCAuX] (X = Cl, $C_6F_4OC_{10}H_{21}$) group produces a slight bathochromic shift (16–25 nm) of the absorption band in the visible region, as a consequence of the stabilization of LUMO relative to HOMO. This behavior is in accordance with the electron withdrawing character of the coordinated isocyanide group on the azulene core [28,48]. In contrast, the transformation of the isocyanide complexes into the corresponding carbene derivatives leads to a hypsochromic shift of 35–38 nm compared to the unfunctionalized azulene. Thus, the carbene complexes display a purple color, which clearly differs from that of the blue isocyanide precursors, and azulene itself.

The molecules under study can be considered as azulene derivatives with a substituent -NCAuX or –N(H)C(NR_2)AuX at the 2-position of the azulene core. In order to gain a deeper insight into the effect of such substituents on the absorption spectra, mainly on the observed color, Density Functional Theory (DFT) calculations were performed on the azulene molecule, two isocyanide gold complexes [AuCl(CNAz)] and [Au($C_6F_4OCH_3$)(CNAz)], and the corresponding carbene gold derivatives [AuCl{C(NHAz)(NMe_2)}] (**1**) and [Au($C_6F_4OCH_3$){C(NHAz)(NMe_2)}] (model for **3**). All DFT calculations were performed using the ORCA software [63]. The ground-state structures of all systems were optimized using the B3LYP functional in combination with the triple -ζ basis set 6-311+G(d,p) for C, H, N, F and Cl, while Au was represented by the aug-cc-pVTZ-pp basis set, including the associated core pseudopotential. Geometry optimizations, as well as TD-DFT calculations, were performed considering dichloromethane solvent effects. For carbene gold(I) complexes, we focused on the most stable stereoisomer, with the optimized geometries in concordance with the structures determined by X-Ray diffraction. Using these optimized geometries, the twenty-first excites states were computed through the TD-DFT approach with several DFT methods (see supplementary information for more details). The calculated electronic absorption energies (ΔE_{TD}), main contributions to the electronic transitions and their oscillator strength (f) as well as the energies and contours of the HOMO and LUMO molecular orbitals are gathered in the supporting material (see Tables S1–S6, and Fig. S27). All the DFT methods employed in this study yielded similar trends. Although transition energies are underestimated, the deviations from the experimental values fall within the range of error expected for the computational protocol employed [64]. Here, we have focused our attention on the absorption band in the visible region, which, as stated above, is essentially attributed to one-electron excitation from HOMO to LUMO.

Fig. 4 displays calculated frontier molecular orbitals and their energies using the B3LYP functional. For the four metal complexes studied, both the HOMO and LUMO orbitals are predominantly localized over the azulene group. The contribution from azulene core exceeds than 96% to HOMO, while the LUMO is also extended over the isocyanide or carbene groups (contribution from these moieties to LUMO orbital lies between 13% for carbene gold derivatives and 24% for isocyanide gold complexes). In the case of the gold isocyanide complexes there is a small contribution from the gold atom, which is not observed in the carbene derivatives (see Fig. 4).

Functionalization at the 2-position of azulene with the isocyanide gold fragments (-NCAuCl and -NCAu$C_6F_4OCH_3$), which are electron-withdrawing groups, causes a notable stabilization of both HOMO and LUMO orbitals (Fig. 4). Meanwhile, the transformation of the isocyanide complexes into the corresponding carbene derivatives produces a destabilization of both frontier orbitals, but this effect is smaller for the HOMO orbitals. Consequently, the HOMO-LUMO gap in the carbene complexes is larger than for the isocyanide derivatives. However, if the

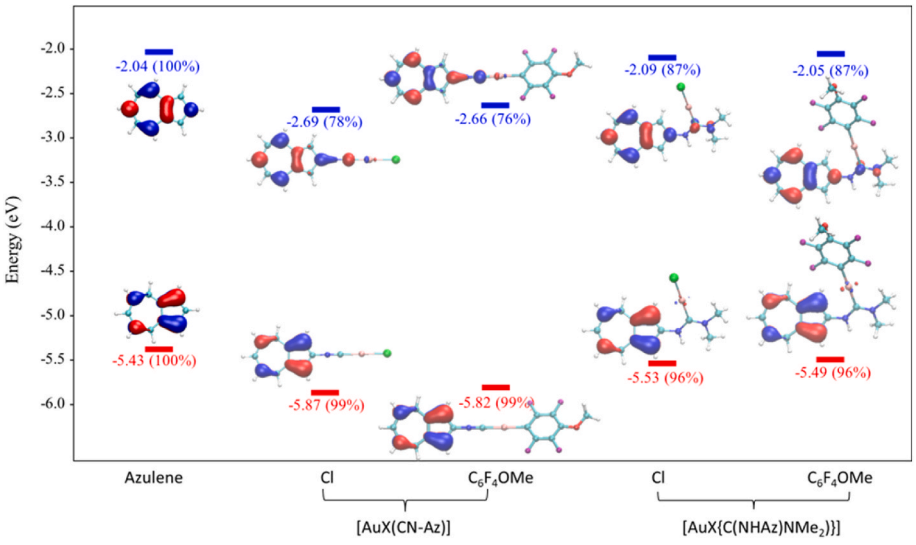

Fig. 4. Frontier molecular orbitals energies along molecular contours (isovalue = 0.05 a.u.). Values in parenthesis represent the percentage contribution from the azulene moiety to the molecular orbital.

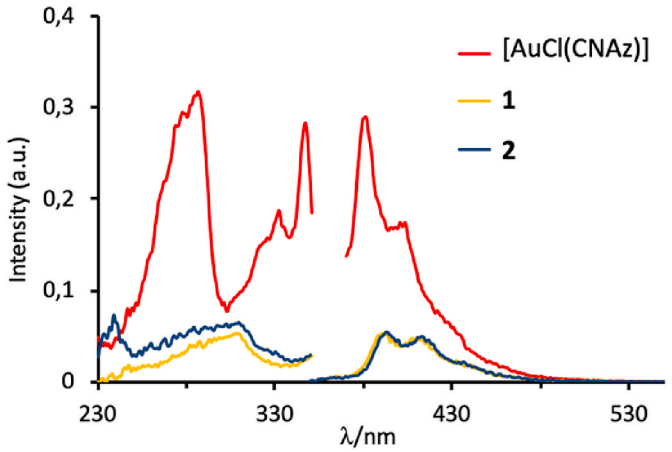

Fig. 5. Selected luminescence spectra recorded in CH_2Cl_2 solution (10^{-5} M) at room temperature.

carbenes and unfunctionalized azulene are compared, the energies of the LUMO orbital of both systems do not display significant energy changes, and the main difference is a slight stabilization of the HOMO orbital in the carbene-gold complexes respect to azulene. As a result, the HOMO-LUMO gap in the azulenic system increases in the order gold isocyanide derivatives < azulene < carbene complexes. Consequently, the gold isocyanide complexes show a blue color, while the carbene derivatives are purple. These results suggest that the isocyanide-gold and carbene-gold fragments behave as substituents in the 2-position of the azulene molecule with a different electron donor/acceptor character. Considering the long-accepted rule that the introduction of an electron-withdrawing substituents in an even position of the azulene molecule produces a bathochromic spectral shift, and an electron-donating group causes the opposite effect, the carbene-gold fragment should act as an electron-donating substituent of the azulene core. Since gold contribution is not observed in the HOMO and LUMO orbitals in the carbene complexes, the –N(H)C(NR_2)AuX group could be formally considered as an amino substituent, whose electron donating character (+M effect) is well known. However, a recent calculation on the related molecule 2-(diphenylamino)azulene at the B3LYP/6–31(d) level [27], leads to a destabilization of the HOMO and LUMO energy levels) with respect to azulene, which is the opposite effect to that found in our carbene-complexes. Consequently, although the functionalization of azulene with a gold diaminocarbene fragment produces a hypsochromic spectral shift, according to DFT calculations the carbene-gold fragment cannot be considered as an electron-donating substituent of the azulene core.

Similar to the free 2-isocyanoazulene ligand and the gold-isocyanide complexes, the carbene derivatives show a very weak emission band in the range 391–395 nm with a well-defined vibronic fine structure (Table 2, and Fig. 5 and S20), which is characteristic of fluorescent azulene derivatives involving S_2–S_0 transitions [48]. The transformation of the isocyanide complexes into the corresponding carbene derivatives mainly leads to a slight bathochromic shift and a smaller Stockes shift. Photoluminescent quantum yields go from 0.4 to 1.39%, while lifetime is in the range 3.64–4.92 ns, close to those found for the starting gold isocyanide and typical for azulene derivatives. In the solid state, even at low temperature (77 K), and in the isotropic liquid the fluorescent emission results deactivated, as observed in the gold isocyanide precursors [48].

Table 2
Emission data for [AuX(CNAz)] (X = Cl, $C_6F_4OC_{10}H_{21}$), [AuCl{C(NHAz)(NR_2)}] (R = Me (**1**) and ^{n}Bu (**2**)) and [Au($C_6F_4OC_{10}H_{21}$){C(NHAz)(NR_2)}] (R = Me (**3**) and ^{n}Bu (**4**)) in dichloromethane (10^{-5} M) at 298 K.

Compound	λ_{ex}/ nm	λ_{em}/ nm	Stokes shift/ nm	τ/ns	φ/%
[AuCl(CNAz)]	287	381	94	2.26	3.14
[Au($C_6F_4OC_{10}H_{21}$)(CNAz)]	299	384	85	3.50	0.5
1	308	391	83	4.25	0.89
2	309	393	84	4.33	0.72
3	305	393	88	3.64	0.40
4	308	395	87	4.92	1.39

4. Conclusions

We have prepared a new series of acyclic diaminocarbene gold(I) complexes via nucleophilic addition of secondary amines to 2-isocyanoazulene gold(I) complexes. The carbene complexes display a deep purple color, which clearly differs from that of the blue isocyanide precursors. In both systems, their intense coloration (purple or blue) is based on one-electron excitation from HOMO to LUMO orbitals that are essentially localized over the azulene group. Although the electronic connection of the azulene core and the isocyanide/carbene substituents is weak, their influence on the electronic spectra is clear. Thus, in contrast to the bathochromic shift observed in the electronic spectra when functionalizing azulene with the gold-isocyanide moiety (electron-withdrawing substituent), the introduction of the gold-carbene fragment in the azulene system leads to a hypsochromic shift. This different electronic behavior is mainly due to the stabilization of the LUMO orbital with respect to the HOMO in the isocyanide complexes compared with azulene, and to the stabilization of the HOMO levels in the carbene derivatives. This work illustrates how the synthetically easy transformation of coordinated isocyanides into acyclic diamino carbenes open new perspectives to color modulation in azulene dyes.

Experimental Section

Materials and general methods. All reactions were carried out under dry nitrogen. The solvents were purified according to standard procedures. Literature methods were used to prepare 2-isocyanoazuleno (CNAz) [45], 1-deciloxi-2,3,5,6- tetrafluorobenzene [65], [AuX(tht)] (X = Cl, $C_6F_4OC_{10}H_{21}$) [66] and [AuX(CNAz)] (X = Cl, $C_6F_4OC_{10}H_{21}$) [48].

Elemental analyses were performed the "Servicio de análisis elemental, CACTI, Universidad de Vigo" with an elemental microanalyzer Fisons Carlo Erba EA1108. IR spectra were recorded on a Perkin-Elmer Frontier spectrometer coupled to a Pike GladiATR-210 accessory. NMR spectra were recorded on Varian 500 instruments in $CDCl_3$ (the assignment key is shown in Fig. 6). MALDI-TOF MS was performed using a Bruker Daltonics autoflex speed instrument equipped with nitrogen laser (340 nm). Positive-ion mode spectra were recorded using the reflective mode. The accelerating voltage was 19 kV. The analytical sample was obtained by mixing the dichloromethane solution of the sample (1 mg/mL) and a solution of the matrix in the same solvent (DCTB, 10 mg/mL) in a 1/5 (vol/vol) ratio. The prepared solution of the sample and the matrix (0.5 μL) was loaded on the MALDI plate and allowed to dry at 23 °C before the plate was inserted into the vacuum chamber of the MALDI instrument. UV–Vis absorption spectra were obtained by means of a Shimadzu UV-2550 spectrophotometer, in dichloromethane (~10^{-5} M). Luminescence spectra were recorded with

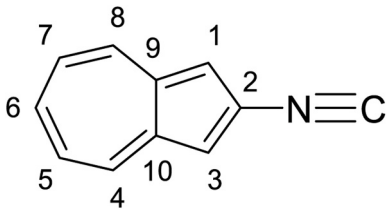

Fig. 6. Assignment key.

a Perkin-Elmer LS-55 spectrometer in CH_2Cl_2 ($\sim 10^{-5}$ M). Photoluminescence quantum yield (QY) was measured with a FLS980 fluorescence spectrometer (Edinburgh Instruments) equipped with an integrating sphere. Fluorescence decays in dichloromethane, at room temperature. Lifetimes were obtained with the Time Correlated Single Photon Counting (TCSPC) and MCP-PMT counter module (TCC2) of the FLS980 spectrometer. Fluorescence decays were analyzed with the method of non-linear least squares iterative deconvolution ant the quality of the fits was judged by the values of the reduced Chi-square (c2) and the autocorrelation function of the residuals using the FAST (Advanced Fluorescence Lifetime Analysis Software) program provided by the equipment. Reconvolution Fit Analysis was used to fit a measured sample decay (red line in Figures) taking into account the IRF Instrument Response Function (black line in Figures). IRF was determined by using Ludox (a scatterer) instead of the sample. DSC was performed using a DSC Q20 from TA Instruments with samples (2−5 mg) sealed in aluminum pans and a scanning rate of 10 °C/min under a nitrogen atmosphere. The transition temperatures are given as peak onsets from the second heating DSC cycle.

Computational details. See Supplementary Data.

Synthesis: general procedure. To a solution of the corresponding isocyanide [AuX(CNAz)] (X = Cl, $C_6F_4OC_{10}H_{21}$) in THF (30 mL) was added the amine HNR_2 (R = Me, n-Bu). After stirring for 30 min at rt, the solution shifts from blue to purple. The solvent was removed under vacuum to give a purple solid, which was recrystallized from dichloromethane/hexane at −20 °C. The obtained purple solid was filtered, washed, and dried.

Compound [AuCl{C(NHAz)(NMe_2)}] (**1**): [AuCl(CNAz)] (30.0 mg, 0.078 mmol) and $HNMe_2$ (107 μL, 0.21 mmol, 2 M THF). Yield: 26 mg, 78 %. Purple solid. IR (cm^{-1}): ν(N–H) 3302 m. ^{1}H NMR (499.72 MHz, $CDCl_3$): δ 8.24 (d, 2H, ^3J = 9.9 Hz, $AzH^{4,8}$), 7.89 (broad, 1H, NH), 7.69 (s, 2H, $AzH^{1,3}$), 7.55 (t, 1H, ^3J = 9.9 Hz, AzH^6), 7.23 (t, 2H, ^3J = 9.9 Hz, $AzH^{5,7}$), 3.70 (s, 3H, NCH_3), 3.18 (s, 3H, NCH_3). $^{13}C\{^1H\}$ NMR (125.67 MHz, $CDCl_3$): δ 190.98 ($C_{carbene}$-Au), 147.14 (C^2_{Az}), 139.70 ($C^{9,10}_{Az}$), 135.89 (H^6-C_{Az}), 135.52 ($H^{4,8}$-C_{Az}), 124.90 ($H^{5,7}$-C_{Az}), 108.08 ($H^{1,3}$-C_{Az}), 49.43, 36.31 (CH_3). Anal. Calcd. for $C_{13}H_{14}N_2ClAu$ (%): C, 36.25; H, 3.28; N, 6.50; found C, 36.52; H, 3.36; N, 6.26. MALDI-TOF MS [$C_{13}H_{14}N_2ClAu(M^+)$]: *m/z*: calculated: 430.0506; found: 430.0495. DSC (Data collected from the first heating cycle): Crystal-Isotropic liquid, 161 °C (5.1 $KJmol^{-1}$).

Compound [AuCl{C(NHAz)(N^nBu_2)}] (**2**): [AuCl(CNAz)] (30.0 mg, 0.078 mmol) and $HNMe_2$ (17 μL, 0.1 mmol). Yield: 30 mg, 75 %. Purple solid. IR (cm^{-1}): ν(N–H) 3255 m. ^{1}H NMR (499.72 MHz, $CDCl_3$): δ 8.24 (d, 2H, ^3J = 9.9 Hz, $AzH^{4,8}$), 7.95 (a, 1H, NH), 7.71 (s, 2H, $AzH^{1,3}$), 7.54 (t, 1H, ^3J = 9.9 Hz, AzH^6), 7.23 (t, 2H, ^3J = 9.9 Hz, $AzH^{5,7}$), 4.05 (t, 2H, ^3J = 7.7 Hz, NCH_2), 3.47 (t, 2H, ^3J = 8.0 Hz, NCH_2), 1.80-1.68 (m, 4H, NCH_2CH_2), 1.51-1.39 (m, 4H, $NCH_2CH_2CH_2$), 1.03 (t, 3H, ^3J = 7.3 Hz, CH_3), 0.98 (t, 3H, ^3J = 7.3 Hz, CH_3). $^{13}C\{^1H\}$ NMR (125.67 MHz, $CDCl_3$): δ 189.93 ($C_{carbene}$-Au), 147.33 (C^2_{Az}), 139.74 ($C^{9,10}_{Az}$), 135.72 (H^6-C_{Az}), 135.35 ($H^{4,8}$-C_{Az}), 124.89 ($H^{5,7}$-C_{Az}), 107.95 ($H^{1,3}$-C_{Az}), 60.59, 47.50 (NCH_2), 31.39, 29.13, 20.46, 19.87 (CH_2), 13.87, 13.75 (CH_3). Anal. Calcd. for $C_{19}H_{26}N_2ClAu$ (%): C, 44.33; H, 5.09; N, 5.44; found C, 44.77; H, 5.13; N, 5.34. MALDI-TOF MS [$C_{19}H_{26}N_2ClAu(M^+)$]: *m/z*: calculated: 514.1445; found: 514.1427. DSC (Data collected from the second heating cycle): Glass-Isotropic liquid, 24 °C.

Compound [Au($C_6F_4OC_{10}H_{21}$){C(NHAz)(NMe_2)}] (**3**): [Au($C_6F_4OC_{10}H_{21}$)(CNAz)] (30.0 mg, 0.046 mmol) and $HNMe_2$ (62 μL, 0.12 mmol, 2 M THF). Yield: 28 mg, 87 %. Purple solid. IR (cm^{-1}): ν(N–H) 3375 m. ^{1}H NMR (499.72 MHz, $CDCl_3$): δ 8.25 (d, 2H, ^3J = 9.8 Hz, $AzH^{4,8}$), 8.02 (broad, 1H, NH), 7.87 (s, 2H, $AzH^{1,3}$), 7.53 (t, 1H, ^3J = 9.8 Hz, AzH^6), 7.24 (t, 2H, ^3J = 9.8 Hz, $AzH^{5,7}$), 4.12 (t, 2H, ^3J = 6.6 Hz, OCH_2), 3.84 (s, 3H, NCH_3), 3.15 (s, 3H, NCH_3) 1.79-1.70 (m, 2H, OCH_2CH_2), 1.48-1.41 (m, 2H, $OCH_2CH_2CH_2$), 1.37-1.23 (m, 12H, CH_2), 0.88 (t, 3H, ^3J = 6.9 Hz, CH_3). $^{13}C\{^1H\}$ NMR (125.67 MHz, $CDCl_3$): δ 207.86 ($C_{carbene}$-Au), 149.80 (m, F_{ortho}-C_{Ar}), 147.90 (C^2_{Az}), 141.01 (m, F_{meta}-C_{Ar}), 139.89 ($C^{9,10}_{Az}$), 135.40 (H^6-C_{Az}), 135.09 ($H^{4,8}$-C_{Az}), 134.56 (m, C_{Ar}-OCH_2), 131.17 (m, C_{Ar}-Au), 124.83 ($H^{5,7}$-C_{Az}), 107.87 ($H^{1,3}$-C_{Az}), 75.03 (O–CH_2), 48.65, 35.86 (NCH_3), 31.89, 29.89, 29.54, 29.33, 25.64, 22.68 (CH_2), 14.11 (CH_3). ^{19}F NMR (470.14 MHz, $CDCl_3$): δ −117.73 (m, 2F, F_{ortho}), −157.45 (m, 2F, F_{meta}). Anal. Calcd. for $C_{29}H_{35}N_2OF_4Au$ (%): C, 49.72; H, 5.04; N, 4.00; found C, 49.86; H, 4.86; N, 4.03. MALDI-TOF MS [$C_{29}H_{35}N_2OF_4Au(M^+)$]: *m/z*: calculated: 700.2346; found: 700.2327. DSC (Data collected from the second heating cycle): Crystal-Isotropic liquid, 107 °C (10.9 $KJmol^{-1}$).

Compound [Au($C_6F_4OC_{10}H_{21}$){C(NHAz)(N^nBu_2)}] (**4**): [Au($C_6F_4OC_{10}H_{21}$)(CNAz)] (30.0 mg, 0.046 mmol) and HN^nBu_2 (10 μL, 0.059 mmol). Yield: 27 mg, 75 %. Purple solid. IR (cm^{-1}): ν(N–H) 3384 d ^{1}H NMR (499.72 MHz, $CDCl_3$): δ 8.25 (d, 2H, ^3J = 9.8 Hz, $AzH^{4,8}$), 8.08 (broad, 1H, NH), 7.90 (s, 2H, $AzH^{1,3}$), 7.52 (t, 1H, ^3J = 9.8 Hz, AzH^6), 7.24 (t, 2H, ^3J = 9.8 Hz, $AzH^{5,7}$), 4.16 (t, 2H, ^3J = 7.8 Hz, NCH_2), 4.13 (t, 2H, ^3J = 6.7 Hz, OCH_2), 3.45 (t, 2H, ^3J = 8.0 Hz, NCH_2), 1.90-1.70 (m, 6H, NCH_2CH_2 y OCH_2CH_2), 1.51-1.27 (m, 18H, CH_2), 1.03 (t, 3H, ^3J = 7.3 Hz, CH_3), 1.00 (t, 3H, ^3J = 7.4 Hz, CH_3), 0.88 (t, 3H, ^3J = 6.9 Hz, CH_3). $^{13}C\{^1H\}$ NMR (125.67 MHz, $CDCl_3$): δ 207.04 ($C_{carbene}$-Au), 149.80 (dm, $^1J_{C\text{-}F}$ = 226 Hz, F_{ortho}-C_{Ar}), 148.12 (C^2_{Az}), 140.97 (dm, $^1J_{C\text{-}F}$ = 248 Hz, F_{meta}-C_{Ar}), 139.95 ($C^{9,10}_{Az}$), 135.20 (H^6-C_{Az}), 134.86 ($H^{4,8}$-C_{Az}), 134.51 (m, CAr-OCH_2), 131.27 (t, $^2J_{C\text{-}F}$ = 58 Hz, C_{Ar}-Au), 124.82 ($H^{5,7}$-C_{Az}), 107.68 ($H^{1,3}$-C_{Az}), 75.04 (O–CH_2), 59.90, 47.27 (NCH_2), 31.91, 31.89, 29.90, 29.56, 29.54, 29.33, 29.30, 25.64, 22.68, 20.52, 19.81 (CH_2), 14.11, 13.88, 13.75 (CH_3). ^{19}F NMR (470.14 MHz, $CDCl_3$): δ −117.63 (m, 2F, F_{ortho}), −157.48 (m, 2F, F_{meta}). Anal. Calcd. for $C_{35}H_{47}N_2OF_4Au$ (%): C, 53.57; H, 6.04; N, 3.57. Found: C, 53.74; H, 5.95; N, 3.57. MALDI-TOF MS [$C_{35}H_{47}N_2OF_4Au(M^+)$]: *m/z*: calculated: 784.3285; found: 784.3302. DSC (Data collected from the first heating cycle): Crystal-Isotropic liquid, 70 °C (30.5 $KJmol^{-1}$).

Supplementary data available

Spectra for the new compounds not included in the text; DSC thermograms; computational data: calculated electronic absorption parameters and frontier molecular orbitals energies in dichloromethane.

CRediT authorship contribution statement

Estela de Domingo: Investigation, Formal analysis. **Manuel Bardají:** Visualization, Formal analysis. **Gregorio García:** Formal analysis. **Silverio Coco:** Supervision, Conceptualization.

Declaration of competing interest

The authors declare that they have no known competing financial interests or personal relationships that could have appeared to influence the work reported in this paper.

Data availability

The research data are included as supplementary material

Acknowledgements

Financial support for this work was provided by grant PID2020-118547GB-I00 funded by MCIN/AEI/10.13039/501100011033s. This research has made use of the high performance computing resources of the Castilla y León Supercomputing Center (SCAYLE, www.scayle.es), financed by the European Regional Development Fund (ERDF). E. D. thanks the Spanish MECD for her FPU contract.

Appendix A. Supplementary data

Supplementary data to this article can be found online at https://doi.org/10.1016/j.dyepig.2024.112149.

References

[1] Xin H, Hou B, Gao X. Azulene-based π-functional materials: design, synthesis, and applications. Acc Chem Res 2021;54:1737–53. https://pubs.acs.org/doi/10.1021/acs.accounts.0c00893.

[2] Salman H, Abraham H, Tal S, Meltzman S, Kapon M, Tessler N, et al. 1,3-Di(2-pyrrolyl)azulene: an efficient luminescent probe for fluoride. Eur J Org Chem 2005;11:2207–12. https://doi.org/10.1002/ejoc.200500012.

[3] López-Alled CM, Sánchez-Fernández A, Edler KJ, Sedgwick AC, Bull SD, McMullin CL, et al. Azulene–boronate esters: colorimetric indicators for fluoride in drinking water. Chem Commun 2017;53:12580–3. https://doi.org/10.1039/C7CC07416F.

[4] Zhou Y, Zou Q, Qiu J, Wang L, Zhu L. Rational design of a green-light-mediated unimolecular platform for fast switchable acidic sensing. J Phys Chem Lett 2018;9:550–6. https://doi.org/10.1021/acs.jpclett.7b03233.

[5] Lvov AG, Bredihhin A. Azulene as an ingredient for visible-light-and stimuli-responsive photoswitches. Org Biomol Chem 2021;19:4460–8. https://doi.org/10.1039/D1OB00422K.

[6] Zhou Y, Zhuang Y, Li X, Ågren H, Yu L, Ding J, et al. Selective dual-channel imaging on cyanostyryl-modified azulene systems with unimolecularly tunable visible near infrared luminescence. Chem Eur J 2017;23:7642–7. https://doi.org/10.1002/Chem201700947.

[7] Dong JX, Zhang HL. Azulene-based organic functional molecules for optoelectronics. Chin Chem Lett 2016;27:1097–104. https://doi.org/10.1016/j.cclet.2016.05.005.

[8] Rao DL, Sun PL, Qin Y, Zhang P, Guo Z-X. Facile fabrication of 1,3-diazaazulene derivative nanowires. Mater Lett 2017;205:182–5. https://doi.org/10.1016/j.matlet.2017.06.075.

[9] Xin H, Gao X. Application of azulene in constructing organic optoelectronic materials: new tricks for an old dog. ChemPlusChem 2017;82:945–56. https://doi.org/10.1002/cplu.201700039.

[10] Xin H, Li J, Ge C, Yang X, Xuea T, Gao X. 6,60 -Diaryl-substituted biazulene diimides for solution-processable high-performance n-type organic semiconductors. Mater Chem Front 2018;2:975–85. https://doi.org/10.1039/c8qm00047f.

[11] Cristian L, Sasaki I, Lacroix PG, Donnadieu B, Asselberghs I, Clays K, et al. Donating strength of azulene in various azulen-1-yl-substituted cationic Dyes: application in nonlinear optics. Chem Mater 2004;16:3543–51. https://doi.org/10.1021/cm0492989.

[12] Migalska-Zalas A, El kouari Y, Touhtouh S. Methodologies for computing UV–VIS spectra and nonlinear properties of azo-azulene derivatives. Opt Mater 2012;34:1639–43. https://doi.org/10.1016/j.optmat.2012.03.021.

[13] Truong MA, Lee J, Nakamura T, Seo JY, Jung M, Ozaki M, et al. Influence of alkoxy chain length on the properties of two-dimensionally expanded azulene-core-based hole-transporting materials for efficient perovskite solar cells. Chem Eur J 2019;25:6647–752. https://doi.org/10.1002/chem.201806317.

[14] Yang L, Zhu Y, Liu J, Chen Y, Wu J, Pang Z, et al. Marked effects of azulenyl vs. naphthyl groups on donor-π-acceptor-π-donor small molecules for organic photovoltaic cells. Dyes Pigments 2021;187:109079. https://doi.org/10.1016/j.dyepig.2020.109079.

[15] Brettle R, Dunmur DA, Estdale S, Marson CM. Synthesis, linear dichroism and mesogenic properties of substituted azulenes. J Mater Chem 1993;3:327–31. https://doi.org/10.1039/JM9930300327.

[16] Estdale SE, Brettle R, Dunmur DA, Marson CM. The azulene ring as a structural element in liquid crystals. J Mater Chem 1997;7:391–401. https://doi.org/10.1039/A606139G.

[17] Fabian KHH, Elwahy AHM, Hafner K. Syntheses of mono-, di- and triethynylazulenes. Tetrahedron Lett 2000;41:2855–8. https://doi.org/10.1016/S0040-4039(00)00308-7.

[18] Mori A, Yokoo M, Hashimoto M, Ujiie S, Diele S, Baumeister U, et al. A novel biaxial smectic liquid crystalline phase formed by rodlike molecules with a 1,3-diazaazulene skeleton. J Am Chem Soc 2003;125:6620–1. https://doi.org/10.1021/ja034569m.

[19] Ito S, Inabe H, Morita N, Ohta K, Kitamura T, Imafuku K. Synthesis of poly(6-azulenylethynyl)benzene derivatives as a multielectron redox system with liquid crystalline behavior. J Am Chem Soc 2003;125:1669–80. https://doi.org/10.1021/ja0209262.

[20] Nakagawa K, Yokoyama T, Toyota K, Morita N, Ito S, Tahata S, et al. Synthesis and liquid crystalline behavior of azulene-based liquid crystals with 6-hexadecyl substituents on each azulene ring. Tetrahedron 2010;66:8304–12. https://doi.org/10.1016/j.tet.2010.08.012.

[21] Akram W, Tagde P, Ahmed S, Arora S, Emran TB, Babalghith AO, et al. Guaiazulene and related compounds: a review of current perspective on biomedical applications. Life Sci 2023;316:121389. https://doi.org/10.1016/j.lfs.2023.121389.

[22] Razus AC, Birzan L, Nae S, Cristian L, Chiraleu F, Cimpeanu V. Azulene-1-azopyridine 1'-oxides. Dyes Pigments 2003;57:223–33. https://doi.org/10.1016/S0143-7208(03)00004-4.

[23] Amir E, Murai M, Amir RJ, Cowart JS, Chabinyc ML, Hawker CJ. Conjugated oligomers incorporating azulene building blocks – seven - vs. five-membered ring connectivity. Chem Sci 2014;5:4483–9. https://doi.org/10.1039/C4SC02210F.

[24] Tang T, Lin T, Wang F, He C. Origin of near-infrared absorption for azulene-containing conjugated polymers upon protonation or oxidation. J Phys Chem B 2015;119:8176–83. https://doi.org/10.1021/acs.jpcb.5b01613.

[25] Zhao C, Wu B, Yang J, Baryshnikov GV, Zhou Y, Ågren H, et al. Large red-shifted NIR absorption in azulenyl- and iodinated-modified BODIPYs sensitive to aggregation and protonation stimuli Dyes. Pigments 2022;197:109867. https://doi.org/10.1016/j.dyepig.2021.109867.

[26] Heilbronner E. Ueber den induktiven effekt der alkylgruppen. Tetrahedron 1963;19:289–313. https://doi.org/10.1016/S0040-4020(63)80022-8.

[27] Tsuchiya T, Wakamiya A, Hamano T, Inoue M, Nakamura T, Mazaki Y. Intense absorption of azulene realized by molecular orbital inversion. Chem Commun 2023;59:10604–7. https://doi.org/10.1039/D3CC02311G.

[28] Shevyakov SV, Li H, Muthyala R, Asato AE, Croney JC, Jameson DM, et al. Orbital control of the color and excited state properties of formylated and fluorinated derivatives of azulene. J Phys Chem A 2003;107:3295–9. https://doi.org/10.1021/jp021605f.

[29] Danzmann S, Liebing P, Engelhardt F, Hilfert L, Edelmann FT. Azulene-1-carboxylate - a new azulene-based building block for coordination polymers. Inorg Chem Commun 2019;99:176–9. https://doi.org/10.1016/j.inoche.2018.11.021.

[30] Cabeza JA, del Río I, Fernández-Colinas JM, García-Alvarez P, Miguel D. Reactivity of indene, fluorene, azulene, and acenaphthylene with a basal-edge-bridged square-pyramidal hexaruthenium dihydride. Organometallics 2007;26:1414–23. https://doi.org/10.1021/om061078c.

[31] Churchill MR. Transition metal complexes of azulene and related ligands. Prog Inorg Chem 1970;11:53–98. https://doi.org/10.1002/9780470166123.ch2.

[32] Töfke S, Behrens U. Azulene as unusual η6-ligand and as η6:η4-Bridge in Mo-complexes. Angew Chem Int Ed Engl 1987;26:147–8. https://doi.org/10.1002/anie.198701471.

[33] Wang F, Lai Y-H, Han MY. Post-coordination of multinuclear transitional metal clusters to azulene-based Polymers: a novel strategy for tuning properties in π-conjugated polymers. Org Lett 2003;5:4791–4. https://doi.org/10.1021/ol0357346.

[34] Lash TD, Colby DA, Graham SR, Ferrence GM, Szczepura LF. Organometallic chemistry of azuliporphyrins: synthesis, spectroscopy, electrochemistry and structural characterization of nickel(II), palladium(II) and platinum(II) complexes of azuliporphyrins. Inorg Chem 2003;42:7326–38. https://doi.org/10.1021/ic030166b.

[35] Lash TD, Pokharel K, Zeller M, Ferrence GM. Iridium(III) azuliporphyrins. Chem Commun 2012;48:11793–5. https://doi.org/10.1039/C2CC37104A.

[36] Stateman LM, Ferrence GM, Lash TD. Rhodium(III) azuliporphyrins. Organometallics 2015;34:3842–8. https://doi.org/10.1021/acs.organomet.5b00433.

[37] Bialek M, Latos-Grazynski L. Merging of inner and outer ruthenium organometallic coordination motifs within an azuliporphyrin framework. Chem Commun 2014;50:9270–2. https://doi.org/10.1039/C4CC04271A.

[38] Colby DA, Ferrence GM, Lash TD. Oxidative metalation of azuliporphyrins with copper(II) salts: formation of a porphyrin analogue system with a unique fully conjugated nonaromatic azulene subunit. Angew Chem Int Ed 2004;43:1346–9. https://doi.org/10.1002/anie.200353189.

[39] Lash TD, Colby DA, El-Beck JA, AbuSalim DI, Ferrence GM. Preparation, structural characterization, assessment of potential antiaromaticity and metalation of 21-oxyazuliporphyrins. Inorg Chem 2015;54:9174–87. https://doi.org/10.1021/acs.inorgchem.5b01587.

[40] Bialek MJ, Bialonska A, Latos-Grazynski L. Oxidation and oxygenation of carbonyl ruthenium(II) azuliporphyrin. Inorg. Chem 2015;54:6184–94. https://doi.org/10.1021/acs.inorgchem.5b00324.

[41] Lash TD. Out of the blue! Azuliporphyrins and related carbaporphyrinoid systems. Acc Chem Res 2016;49:471–82. https://doi.org/10.1021/acs.accounts.5b00523.

[42] Holovics TC, Robinson RE, Weintrob EC, Toriyama M, Lushington GH, Barybin MV. The 2,6-diisocyanoazulene Motif: synthesis and efficient mono- and heterobimetallic complexation with controlled orientation of the azulenic dipole. J Am Chem Soc 2006;128:2300–9. https://doi.org/10.1021/ja053933+.

[43] DuBose DL, Robinson RE, Holovics TC, Moody DR, Weintrob EC, Berrie CL, et al. Interaction of mono- and diisocyanoazulenes with gold Surfaces: first examples of self-assembled monolayer films involving azulenic scaffolds. Langmuir 2006;22:4599–606. https://doi.org/10.1021/la0532050.

[44] Maher TR, Spaeth AD, Neal BM, Berrie CL, Thompson WH, Day VW, et al. Linear 6,60 -biazulenyl framework featuring isocyanide termini: synthesis, structure, redox behavior, complexation, and self-assembly on Au(111). J Am Chem Soc 2010;132:15924–6. https://doi.org/10.1021/ja108202d.

[45] Robinson RE, Holovics TC, Deplazes SF, Powell DR, Lushington GH, Thompson WH, et al. Five possible isocyanoazulenes and electron-rich complexes Thereof: a quantitative organometallic approach for probing electronic inhomogeneity of the azulenic framework. Organometallics 2005;24:2386–97. https://doi.org/10.1021/om0502180.

[46] Fathi-Rasekh M, Rohde GT, Hart MD, Mason DH, Nakakita T, Zatsikha YV, et al. Positional isomers of isocyanoazulenes as axial ligands coordinated to ruthenium (II) tetraphenylporphyrin: fine-tuning redox and optical profiles. Inorg Chem 2019;58:9316–25. https://doi.org/10.1021/acs.inorgChem9b1030.

[47] Applegate JC, Okeowo MK, Erickson NR, Neal BM, Berrie CL, Gerasimchuk NN, et al. First π-linker featuring mercapto and isocyano anchoring groups within the same molecule: synthesis, heterobimetallic complexation and self-assembly on Au (111). Chem Sci 2016;7:1422–9. https://doi.org/10.1039/c5sc04017e.

[48] Domingo E, Barcenilla M, Martín-Alvarez JM, Miguel JA, Coco S. The 2-isocyanoazulene-gold(I) fragment as a versatile element for organometallic dyes and liquid crystals. Dyes Pigments 2020;176:108195. https://doi.org/10.1016/j.dyepig.2020.108195.

[49] Kinzhalov MA, Luzyanin KV. Reactivity of acyclic diaminocarbene ligands. Coord Chem Rev 2019;399:213014. https://doi.org/10.1016/j.ccr.2019.213014.

[50] Bartolomé C, Ramiro Z, Peñas-Defrutos MN, Espinet P. Some singular features of gold catalysis: protection of gold(I) catalysts by substoichiometric agents and

associated phenomena. ACS Catal 2016;6:6537–45. https://doi.org/10.1021/acscatal.6b01825.
[51] Bartolomé C, Ramiro Z, García-Cuadrado D, Pérez-Galán P, Bour C, Raducan M, et al. Nitrogen acyclic gold(I) carbenes: excellent and easily accessible catalysts in reactions of 1,6-enynes. Organometallics 2010;29:951–6. https://doi.org/10.1021/om901026m.
[52] Harris RJ, Widenhoefer RA. Gold carbenes, gold-stabilized carbocations, and cationic intermediates relevant to gold-catalysed enyne cycloaddition. Chem Soc Rev 2016;45:4533–51. https://doi.org/10.1039/C6CS00171H.
[53] Wang T, Hashmi ASK. 1,2-Migrations onto gold carbene centers. Chem Rev 2021;121:8948–78. https://doi.org/10.1021/acs.chemrev.0c00811.
[54] He Y, Huang Z, Wu K, Ma J, Zhou YG, Yu Z. Recent advances in transition-metal-catalyzed carbene insertion to C–H bonds. Chem Soc Rev 2022;51:2759–852. https://doi.org/10.1039/D1CS00895A.
[55] Nugegoda D, Tzouras NV, Nolan SP, Delcamp JH. N-Heterocyclic carbene gold complexes in a photocatalytic CO2 reduction reaction. Inorg Chem 2022;61:18802–9. https://doi.org/10.1021/acs.inorgchem.2c03487.
[56] Aliaga-Lavrijsen M, Herrera RP, Villacampa MD, Gimeno MC. Efficient gold(I) acyclic diaminocarbenes for the synthesis of propargylamines and indolizines. ACS Omega 2018;3:9805–13. https://doi.org/10.1021/acsomega.8b01352.
[57] Baker MV, Barnard PJ, Berners-Price SJ, Brayshaw SK, Hickey JL, Skelton BW, et al. Synthesis and structural characterisation of linear Au(I) N-heterocyclic carbene complexes: new analogues of the Au(I) phosphine drug Auranofin. J Organomet Chem 2005;690:5625–35. https://doi.org/10.1016/j.jorganChem2005.07.013.
[58] Niu W, Chen X, Tan W, Veige AS. N-heterocyclic carbene–gold(I) complexes conjugated to a leukemia-specific DNA aptamer for targeted drug delivery. Angew Chem Int Ed 2016;55:8889–93. https://doi.org/10.1002/anie.201602702.
[59] Sen S, Hufnagel S, Maier EI, Aguilar I, Selvakumar J, DeVore JE, et al. Rationally designed redox-active Au(I) N-heterocyclic carbene: an immunogenic cell death inducer. J Am Chem Soc 2020;142:20536–41. https://doi.org/10.1021/jacs.0c09753.
[60] Hussaini SY, Haque RA, Razali MR. Recent progress in silver(I)-, gold(I)/(III)- and palladium(II)-N- heterocyclic carbene complexes: a review towards biological perspectives. J Organomet Chem 2019;882:96–111. https://doi.org/10.1016/j.jorganchem.2019.01.003.
[61] Visbal R, Gimeno MC. N-heterocyclic carbene metal complexes: photoluminescence and applications. Chem Soc Rev 2014;43:3551–74. https://doi.org/10.1039/C3CS60466G.
[62] Amouri H. Luminescent complexes of platinum, iridium, and coinage metals containing N-heterocyclic carbene ligands: design, structural diversity, and photophysical properties. Chem Rev 2023;123:230–70. https://doi.org/10.1021/acs.chemrev.2c00206.
[63] Neese F. The ORCA program system. WIREs Comput Mol Sci 2012;2:73–8. https://doi.org/10.1002/wcms.81.
[64] Jacquemin D, Wathelet V, Perpète EA, Adamo C. Extensive TD-DFT benchmark: singlet-excited states of organic molecules. J Chem Theor Comput 2009;5:2420–35. https://doi.org/10.1021/ct900298e.
[65] Bayón R, Coco S, Espinet P. Twist-grain boundary phase and blue phases in isocyanide gold(I) complexes. Chem Mater 2002;14:3515–8. https://doi.org/10.1021/cm020246y.
[66] Usón R, Laguna A, Laguna M. (Tetrahydrothiophene)Gold(I) or gold(III) complexes. Inorg Synth 1989;26:85–91. https://doi.org/10.1002/9780470132579.ch17.